Full Paper

DNA Assisted Assembly of Multisegmented Nanowires

Joun Lee,[a] *Aijun A. Wang,*[b] *Youngwoo Rheem,*[a] *Bongyoung Yoo,*[a] *Ashok Mulchandani,*[a] *Wilfred Chen,*[a]* *Nosang V. Myung*[a]*

[a] Department of Chemical and Environmental Engineering and Center for Nanoscale and Engineering, University of California-Riverside, Riverside, CA 92521, USA
[b] Office of Environmental Health Hazards Assessment, California Environmental Protection Agency, Sacramento, CA 95812, USA
*e-mail: wilfred@engr.ucr.edu, myung@engr.ucr.edu

Received: July 9, 2007
Accepted: August 7, 2007

Abstract
This work demonstrates a highly specific and selective assembly of multisegmented nanowires on prepatterned gold electrodes using DNA hybridization. Multisegmented Au/Pd/Au nanowires were synthesized using template-directed electrodeposition. Two complementary single-stranded DNAs modified with thiol tags adsorb on gold electrodes and gold segments of nanowires, and enable the nanowires to assemble across electrodes. The assembled nanowires show ohmic contact with minimum contact resistance. Using these nanowires, the temperature dependent electrical resistance and the sensing performance toward hydrogen were investigated. The temperature coefficient of resistance of nanowires was lower than bulk polycrystalline counterpart, because of higher electron scattering at the surface and grain boundaries of nanowires. The nanowires were sensitive toward hydrogen gas at room temperature with a detection limit of 0.5%.

Keywords: DNA, Nanowire, Multisegmented nanowires, Assembly, Hydrogen, Gas sensor

DOI: 10.1002/elan.200704000

1. Introduction

One-dimensional nanostructures including nanowires and nanotubes are becoming increasingly important as building blocks of nanodevices, because of their unique electronic, physical, and optical properties that can be precisely controlled by controlling their shapes and sizes [1, 2]. However, exploiting the full potential of nanostructures and their characteristics has been limited by the inability to spatially manipulate and address these nanoentities [3]. Efficiently controlled assembly of nanostructures into more complex structures is necessary for realizing applications such as nanoelectronics, spintronics, optoelectronics, sensors, and thermoelectric devices.

There have been several methods for assembling the nanostructures in complex architectures, which include during- and post-growth electric field assisted alignment [4–6], Langmuir-Blodgett methods [7, 8], microfluidic techniques [9], and magnetic assembly [10–13]. Biorecognition-directed assembly is an attractive method to assemble nanostructures into functional devices because of the highly specific nature offered by biomolecules such as proteins and deoxyribonucleic acid (DNA). DNA is particularly attractive because the interaction between complementary DNA is very specific and reversible, enabling highly controlled assembly of nanostructures. DNA can be easily synthesized with different lengths, sequences, and functional groups. In addition, the sequence selectivity of DNA hybridization provides a way to create complex structures by incorporating multiple different sequence pairs. These properties in concert with the site-specific DNA adsorption and the reversibility of the hybridization have been exploited for the assembly of Au nanoparticles functionalized with thiolated single-stranded DNA (ssDNA) onto a prepatterned surface [14–18]. Selective assembly of gold nanoparticles on a defined gold pattern was demonstrated by passivating the rest of the surface with PEG-silane [19]. Recently, the direct assembly of gold nanowires on complementary surfaces has been reported [20]. It is easy to envision that even multisegmented nanowires containing gold segments at each end can be selectively assembled using the DNA-assisted assembly method.

In this paper, we demonstrate a facile way to assemble functional multisegmented nanowires in a spatially controlled manner using DNA hybridization. This assembly technique was exploited for bridging multisegmented Au/Pd/Au nanowires across two gold electrodes by the selective DNA hybridization. The properties of the nanowires were investigated by measuring temperature dependent electrical property and sensing performance toward hydrogen.

2. Experimental

2.1. Nanowire Fabrication

Nanowires with diameter of approximately 200 nm were synthesized using template-directed electrodeposition. Anodized alumina (Anodisc 13 from Whatman, Inc. with a nominal pore diameter of 200 nm) was used as a scaffold. A gold layer with a thickness of approximately 500 nm was sputtered on one side of the template to serve as the seed layer. The template was fixed to a glass support with the seed layer face down using double-sided conductive copper tape. The conductive copper tape was also used as a lead to the glass support. The entire sample, except for the middle of the template and the end of the copper tape lead, was masked with an insulator (Microstop, Pyramid Plastics, Inc.).

The Au/Pd/Au multisegmented nanowires were synthesized by sequential electrodeposition of gold, palladium, and gold under potentiostatic conditions. The lengths of different segments were controlled by adjusting deposition times at fixed deposition potentials. Platinum-coated titanium bars and saturated calomel electrodes (SCE) were used as anodes and reference electrodes, respectively, for all deposition. The gold segments were electrodeposited from ready-to-use cyanide-free gold electrolytes (RTU-25, Technic, Inc.) at 60 °C. The deposition potential was fixed at − 0.5 V vs. SCE, which resulted in an average current density of − 1.2 mA cm^{-2}. The pH of the electrolyte was maintained at 7.25. The current efficiency of the gold electrodeposition was approximately 100 %. The palladium segments were electrodeposited at room temperature from alkaline chloride electrolytes with ammonium ions as complexing agents. The electrolyte solution had a composition of 0.047 M $Pd(NH_3)_4Cl_2$ and 0.1 M NH_4Cl at pH of 7.02. The deposition potential was fixed at − 0.8 V vs. SCE, which resulted in an average current density of − 3.2 mA cm^{-2}. At this deposition potential and temperature, the current efficiency of palladium electrodeposition was approximately 30%. For all depositions, electrolyte solutions were magnetically agitated using 1 inch stir bar at 200 rpm in 100 mL beaker, and deposition potentials were controlled by a multichannel EG&G PAR VMP2 potentio/galvanostat.

After electrodeposition, the nanowire-embedded template was removed from the substrate followed by mechanical removal of the gold seed layer. The nanowire-embedded template was sonicated in acetone to remove the adhesives smeared by the copper tape. The adhesives on the template surface could hinder the dissolution of the alumina template and also remained in the final nanowire solution as contaminants. The nanowire embedded template was then immersed in 5 M NaOH for 24 h. at 60 °C for selective removal of template. The suspended nanowires were thoroughly washed with nanopure water for three times. Finally, the nanowires were stored in 1 mL of nanopure water.

2.2. Microfabrication of Gold Electrodes

The gold electrodes were microfabricated on silicon substrate using standard lithographic patterning. Using chemical vapor deposition (CVD), one micron thick SiO_2 film was first deposited on a (100) oriented silicon wafer to insulate the substrate. After photo lithographically defining the electrode area, a Cr adhesion layer and a ca. 3000 Å-thick Au layer were e-beam evaporated. Finally, the electrodes were defined using lift-off techniques. The gap distance between electrodes was fixed at 3 μm.

2.3. DNA Functionalization

Figure 1 shows the schematic illustration of DNA functionalization and assembly of multisegmented nanowires on microfabricated gold electrodes. The protocols for DNA functionalization were adopted in part from Papra et al. for passivating the silicon dioxide surface with PEG silane, and from Kannan et al. for functionalizing the nanowires and gold electrodes with DNAs [19, 21]. The base sequences of the complementary DNAs (i.e. DNA_1 and DNA_2) used for this study were:

DNA_1: 5′-SH-C_6-TTTTTTTTTTTTTTTTTTT AAT ATT GAT AAG GAT

DNA_2: 5′-SH-C_6-TTTTTTTTTTTTTTTTTTT ATC CTT ATC AAT ATT

DNA_1 and DNA_2 were used to functionalize the nanowires and the gold electrode surface, respectively. The first 20 bases from 5′ end function as spacers and the rest 15 bases as linkers that hybridize to the complementary base sequences.

The thiolated DNAs (Integrated DNA Technologies) were dissolved in 100 μL of a 0.1 M dithiothreitol (DTT) solution, and kept at room temperature for 12 hours in order to reduce the disulfide bonds. The solution was diluted to a final volume 1 mL with nanopure water, and ran through a NAP-10 column (GE Healthcare Bio-Sciences AB) to remove the DTT from the DNA solution. The final volume and the concentration of the DNA solutions after being eluted were approximately, 1.5 mL and 100 μM, respectively. The DNA solutions were kept frozen to prevent the formation of disulfide bonds.

A silicon chip with patterned gold electrodes was first cleaned with Piranha (70 vol% sulfuric acid and 9 vol% hydrogen peroxide in water) for 20 minutes. The chip was then washed three times in nanopure water and dried at 90 °C for 10 minutes. A PEG-toluene solution consisting of 0.2 vol% PEG-silane + 0.08 vol% HCl + 99.97 vol% toluene was sonicated in medium power for 10 minutes and transferred to a clean glass beaker. The chip was placed in the PEG-toluene solution for 1 hour and washed once in toluene, once in ethanol and finally in nanopure water. 20 μL of DNA_2 solution was added to cover on the gold electrodes for 12 hours. The chip was rinsed with 0.1 vol%

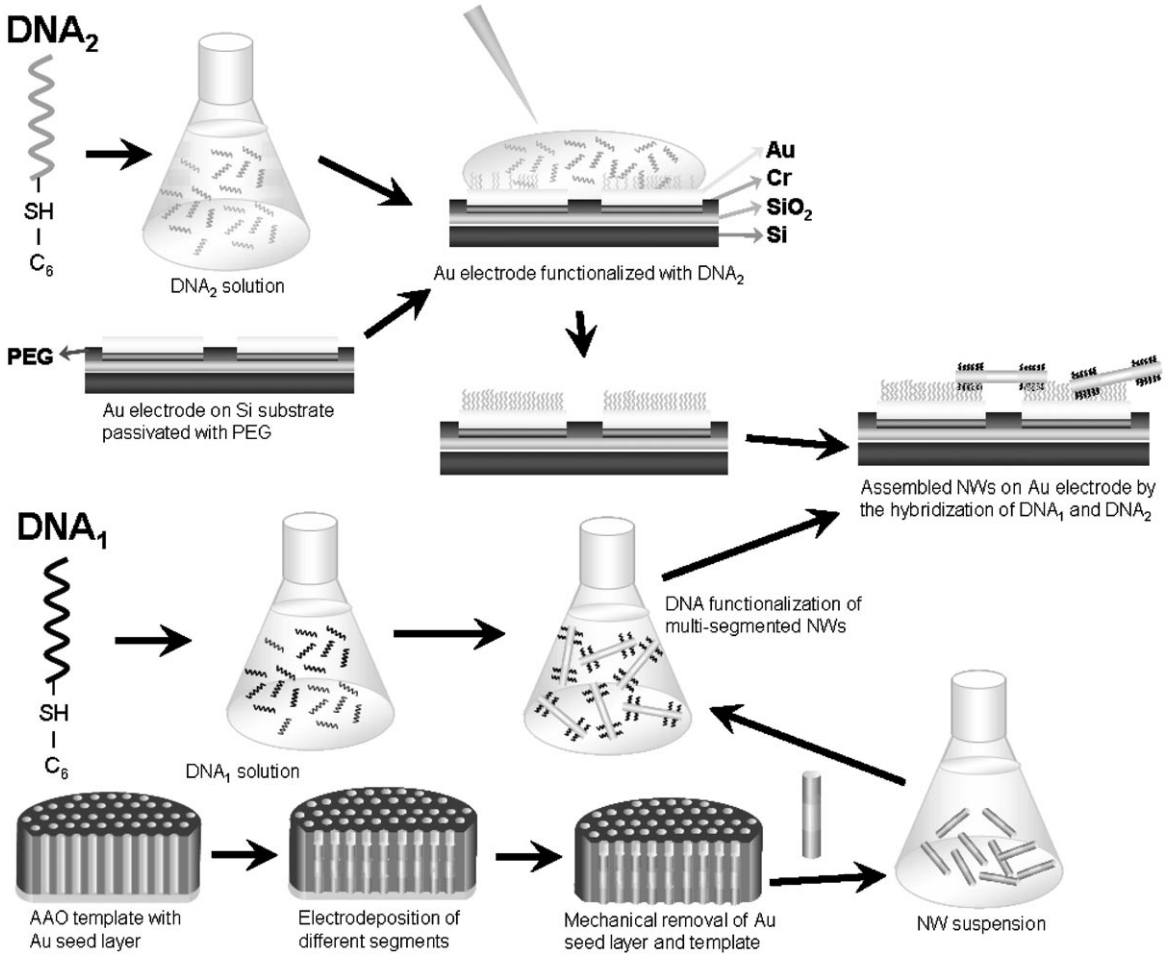

Fig. 1. Schematic illustration of DNA assisted assembly of nanowires. The upper part of the schematic illustrates the DNA functionalization of gold electrodes with DNA_2, and the lower part of the schematic illustrates the DNA functionalization of the nanowires with complimentary DNA. After the DNA functionalization, the nanowires are assembled across the gold electrodes.

Tween-20 followed by nanopure water, and placed in 1 mM mercaptohexanol (MCH) for 1 hour. MCH was used to assist the single-stranded DNAs (ssDNA) to stand vertically on the surface. Finally, the chip was washed with nanopure water for 2 minutes.

The nanowires were suspended in 200 μL of a 14.7 mM phosphine ligand solution and incubated for 12 hours on a rotator. 100 μL of DNA_1 solution was added to the nanowire suspension and incubated for another 12 hours. NaCl was added to the solution to a final concentration of 50 mM to aid the oligonucleotides to stand vertically on the nanowire surfaces. After the functionalization, the solution was centrifuged at 14 000 rpm for 10 minutes and the supernatant containing the unreacted ssDNAs was removed. The DNA functionalized nanowires were re-suspended in 500 μL of 10 mM phosphate buffer (PB) and 0.3 M NaCl solution.

2.4. DNA Hybridization

The ssDNA functionalized chip was incubated in a solution of the nanowires conjugated to the complementary oligonucleotides for 12 hours to allow the hybridization between complementary ssDNAs. After the hybridization, the chip was washed for 2 minutes with 0.1 vol% Tween-20 in 10 mM PB and 0.3 M NaCl solution, followed by 10 mM PB and 0.3 M NaCl solution.

2.5. Morphology, Electrical Properties, and Hydrogen Gas Sensing

The morphology of Au/Pd/Au nanowires was examined by high resolution optical video microscope (KH-3000, Hirox, Inc.) and scanning electron microscopy (Philips model # XL30-FEG). The crystal structure of Au/Pd/Au nanowires was determined using X-ray diffractometer (D8 Advance Diffractometer by Bruker using Cu K_α radiation). The temperature dependent electrical properties of Au/Pd/Au nanowires were characterized using Physical Property Measurement System (PPMS). The $I-V$ characteristics of Au/Pd/Au nanowires were analyzed using semiconductor parameter analyzer (HP model # 4155A).

The gold electrodes with assembled Au/Pd/Au nanowires were wire-bonded to a chip carrier. A 1.3 cm^3 sealed glass

chamber with inlet and outlet ports for gas flow-through was positioned over the sensor chip. The circuits were connected to a semiconducting parameter analyzer to continuously monitor the voltage change at a constant current of 200 μA. The electrical resistance of the sensor was determined by applying Ohm's law based on the measured voltages. The gas flow rates of hydrogen and dry air were regulated by mass flow controllers (Alicat Scientific Incorporated, Tucson, AZ). All experiments were conducted at room temperature with hydrogen (purity: 99.998%) diluted in dry air (purity: 99.998%) at a flow rate of 150 std. cm^3 min^{-1}.

3. Results and Discussion

Figure 2 shows the optical cross-sectional images of Au/Pd/Au nanowires. The lengths of segments were 2.8/2.6/2.6 μm, respectively. Presence of two different metal segments was clearly indicated by the two distinct colors. The length of each segment was designed to match the microgap distance between the two bridging electrodes. Electrodeposition was controlled at a relatively low cathodic potential, which consequently applied low current density (-1.24 mA cm^{-2} for gold, -3.2 mA cm^{-2} for palladium), to ensure the length uniformity of nanowires. Figure 2B shows single Au/Pd/Au nanowires well-dispersed in nanopure water after the dissolution of alumina template with sodium hydroxide.

Figure 3 shows the X-ray diffraction pattern of Au/Pd/Au nanowires after the removal of alumina template. The nanowires were polycrystalline and show face centered cubic (FCC) structure. The intensity ratio of I_{111}/I_{200} for gold segments was 2.4, which indicated that the gold segments have preferred the orientation along [111] direction. The palladium segments have also preferred the orientation along [111] direction. Using Debye-Scherrer's equation, the mean grain sizes of gold and palladium segments were determined to be 28.5 and 34.3 nm, respectively.

To verify that the DNA-assisted assembly can be extended to multisegmented nanowires, the ability to deposit Au/Pd/Au segmented nanowires onto plain gold surfaces was studied. On the same chip, one gold surface was functionalized with DNA_2 and the other gold surface was not functionalized as a control. The gold surfaces were

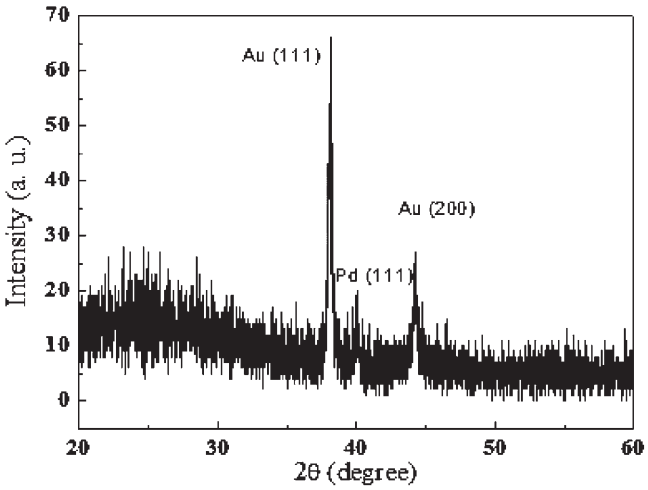

Fig. 3. X-ray diffraction pattern of Au/Pd/Au nanowires.

incubated with a drop of the Au/Pd/Au nanowire solution that was functionalized with DNA_1. After washing the gold surfaces, observable nanowires deposition was detected only on the gold surface functionalized with DNA_2 (Fig. 4A and B). The PEG groups presented on the silicon dioxide surfaces prevent any nonspecific binding of nanowires [22, 23].

Previously Mbindyo et al. [20] have demonstrated the DNA hybridization of gold nanowires on gold surfaces. The group investigated surface coverage of 6 μm-long gold nanowires with a diameter of 200 nm. They achieved a surface density of $(9 \pm 2) \times 10^5$ N W s cm^{-2} by using a 36mer DNA oligo pair functionalized on the nanowires and surfaces. The surface coverage of our Au/Pd/Au segmented nanowires, which were 8 μm in length and 200 nm in diameter, was 3.2×10^5 N W s cm^{-2}. This result indicates that the non DNA-binding palladium middle segment has no adverse effect on DNA hybridization and the same order of magnitude of nanowire coverage could be achieved.

Similar hybridization experiments were performed on a four-interdigitated gold electrode to further investigate the directed positioning of nanowires across electrodes. Using the same strategy of hybridization on two different interdigitated gold electrodes, we confirmed the same results

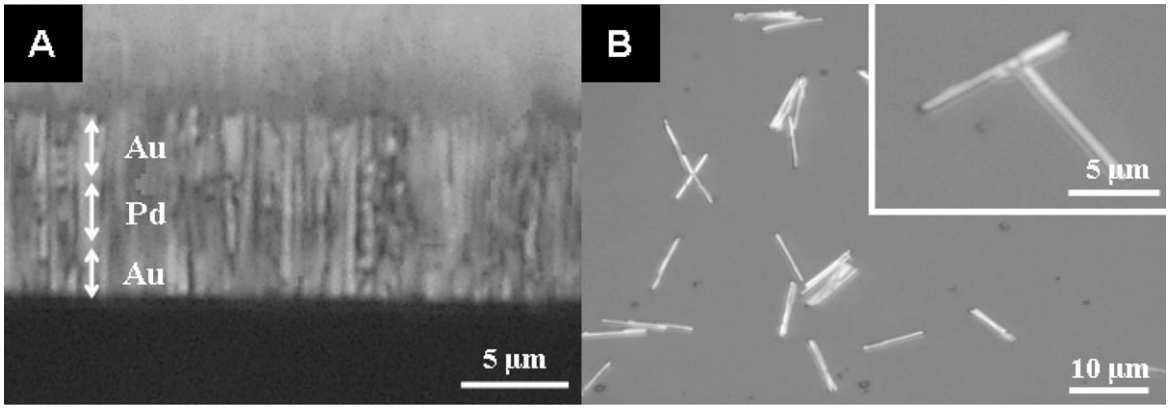

Fig. 2. Optical images of multisegmented Au/Pd/Au nanowires embedded in alumina template (A) and dispersed nanowires (B).

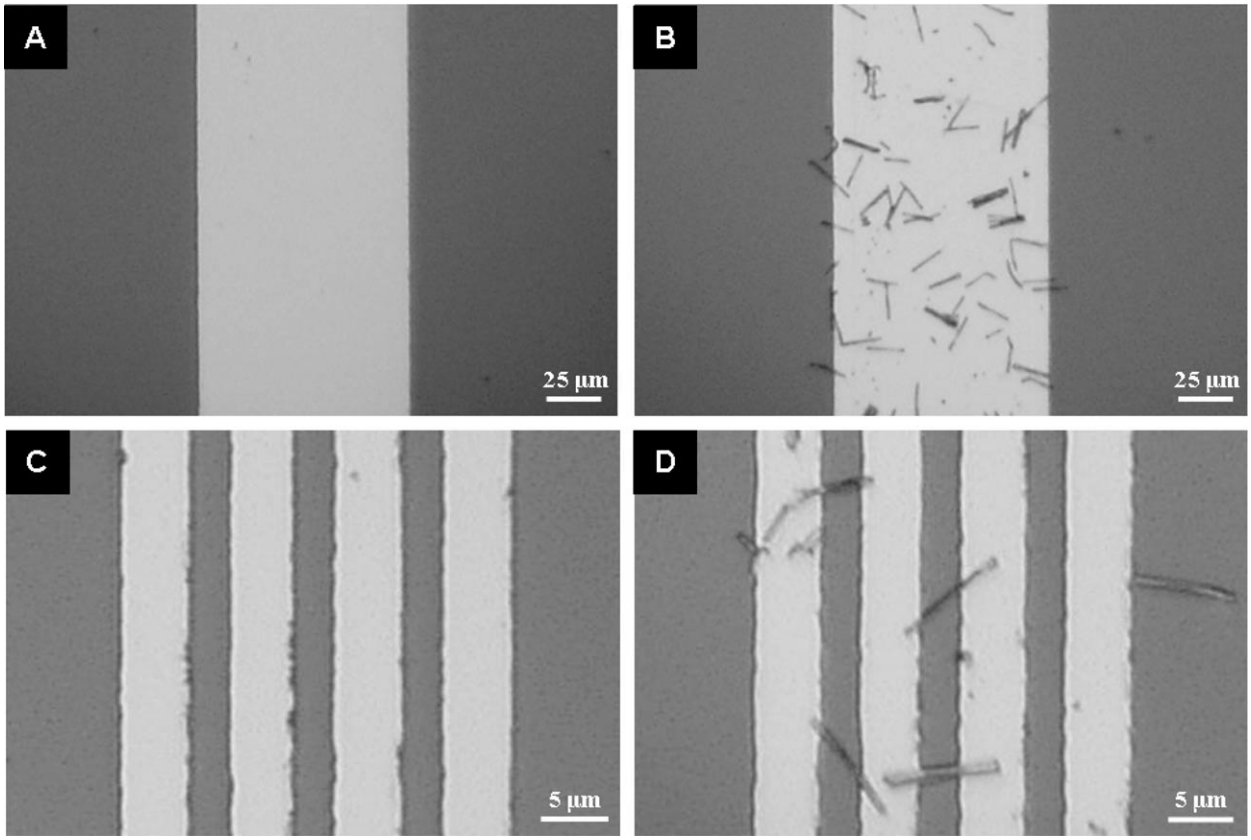

Fig. 4. Assembly of nanowires on gold electrodes A) unfunctionalized gold surface incubated with DNA_1 functionalized nanowires (control), B) DNA_2 functionalized gold surface incubated with DNA_1 functionalized nanowires, C) unfunctionalized interdigitated gold electrodes with DNA_1 functionalized nanowires (control), and D) DNA_2 functionalized interdigitated electrodes with DNA_1 functionalized nanowires.

showing no nanowires on the non-functionalized electrode (Fig. 4C), and approximately 30% of nanowires were assembled across DNA-functionalized electrodes (Fig. 4D). In accordance with our design of the nanowire, only the gold segments were interacting with the gold electrodes via DNA hybridization while the palladium segment remained in the middle of the microgap (Fig. 4D). The yield of assembly can be further improved by reducing the width of electrodes similar to the length of gold segments to minimize the probability of nanowires deposited on one electrode. In addition, integrated magnetic segment (e.g., Ni, Co, or Fe) within nanowires can provide directionality upon applied external magnetic field [12].

Figure 5A shows a tilted SEM image of the DNA assisted Au/Pd/Au nanowire bridging two microfabricated gold electrodes. Line scanning of the EDAX confirmed that the palladium segment is located in the middle of the microgap, which indicated that gold segments were interacting with the gold electrodes (Fig. 5B).

The room temperature $I-V$ characteristic of assembled Au/Pd/Au nanowires was measured by sweeping the voltage from -10 mV to 10 mV (Fig. 6A). 66% of observed assembled nanowires showed ohmic behavior, with resistance ranging from 66 to 178 Ω at room temperature (Fig. 6B). Since the double-stranded DNA (dsDNA) layer between the electrodes and the nanowire is thinner (≈11 nm) and soft, the ohmic contact between nanowire and electrodes might be attributed to direct contact between them. The lowest resistivity of single assembled nanowire was approximately 126 Ωcm, which was greater than bulk palladium (10.5 Ωcm). Higher electrical resistivity of assembled nanowires might be attributed to greater electron scattering at the wire surfaces and the grain boundaries [24–28].

Temperature dependent electrical resistance of Au/Pd/Au nanowire was measured from 10 to 320 K in increasing step. As the temperature was increased, the resistance of nanowire monotonically increased. For a detailed analysis, the temperature coefficient of resistance (TCR) was calculated using

$$TCR = \frac{1}{R_0}\frac{\Delta(R-R_0)}{\Delta(T-T_0)} \quad (1)$$

where R is the resistance at temperature, T, and R_0 is the resistance at T_0, which is 300 K. Since, gold segments are assembled on top of electrodes, and have much lower electrical resistivity than the palladium segment, the majority of electrical resistance is expected to come from the palladium segment. Figure 7 shows the comparison of the

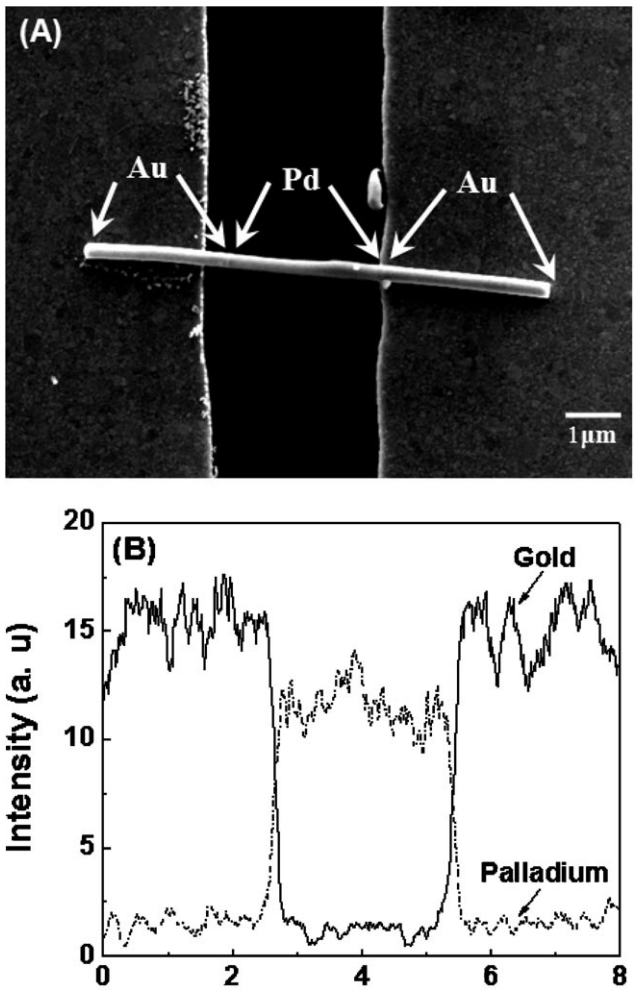

Fig. 5. SEM image (A) and EDX line scan (B) of an assembled Au/Pd/Au nanowire between electrodes.

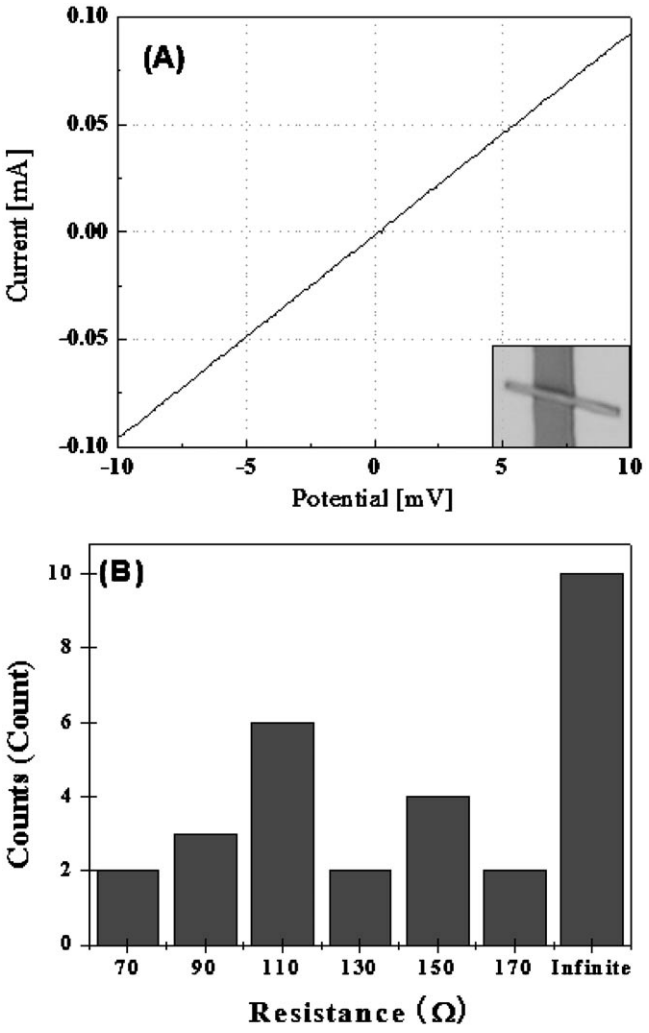

Fig. 6. Room temperature $I-V$ characteristic of a single Au/Pd/Au nanowire bridging microfabricated gold electrodes. The gap distance between electrodes was approximately 3 μ. Inset: optical image of the assembled nanowire.

normalized resistance of multisegmented nanowires versus bulk polycrystalline palladium, and DNA templated palladium nanowires [27]. The diameter of DNA templated palladium nanowires was approximately 60 nm. The TCR of the multisegmented nanowire was 0.0027 K^{-1} compared to 0.0007 K^{-1} and 0.0034 K^{-1} for the DNA templated Pd nanowire and bulk palladium, respectively, at 290 K. As expected, the TCR of multisegmented nanowires (200 nm in diameter) lies between that of the DNA templated Pd nanowire (60 nm in diameter) and bulk palladium. Lower TCR of nanowire compared to the bulk counterpart is caused by an increase in the volume fraction of interface scattering sites with a decrease of nanowire diameter [30].

The functionality of the DNA-assisted assembled nanowires was demonstrated by utilizing the palladium middle segment for hydrogen sensing, since the resistance of palladium increases when it is exposed to hydrogen. The sensing performance of nanowire was characterized as a function of hydrogen concentration at room temperature. Figure 8 shows that the sensor resistance increases rapidly in response to a hydrogen injection, and returns to the baseline resistance upon purging with dry air. The inset of Figure 8

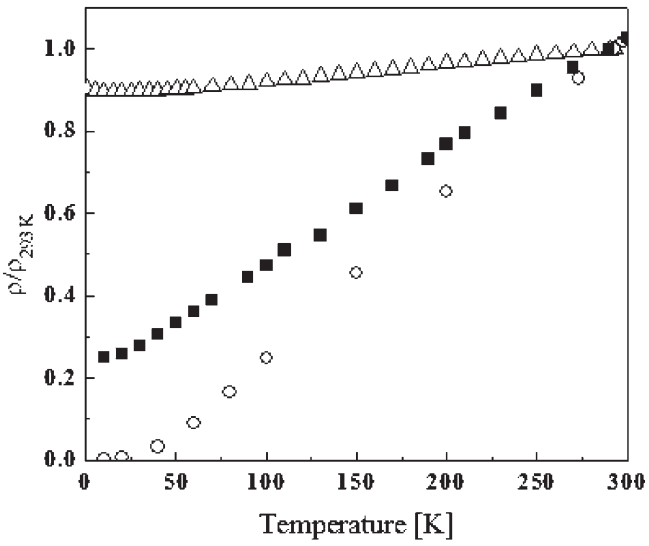

Fig. 7. Normalized resistance of Au/Pd/Au nanowires (■), bulk palladium (○), and DNA templated palladium nanowire [29] (△) as a function of temperature.

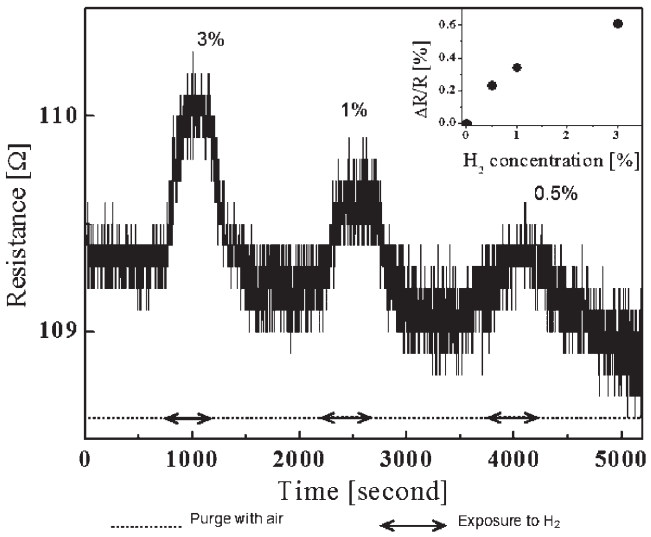

Fig. 8. Resistance versus time in the presence of various hydrogen gas concentrations (3%, 1%, and 0.5 vol%). Inset: the hydrogen sensitivity of assembled nanowire as a function of hydrogen concentration. The arrows indicate the exposure to hydrogen.

shows the sensitivity of the sensor, which was defined as the relative resistance change over the initial resistance. The assembled nanowires responded to hydrogen with a detection limit of 0.5 vol% at room temperature. The sensitivity ($\Delta R/R$) of assembled nanowires increased linearly with an increase in hydrogen concentration, and was comparable to previously reported results [31, 32]

4. Conclusion

In summary, we demonstrated a facile method of site-specific assembling of Au/Pd/Au nanowires on microfabricated gold electrodes using DNA hybridization. The surface coverage of multisegmented nanowires was similar to gold nanowires, which indicates that the non DNA-binding palladium middle segment has no adverse effect on DNA hybridization. The assembled nanowires show ohmic contact with minimum contact resistance. The temperature dependent electrical resistances show that the majority of electron scattering occurred at the surface and grain boundaries. The assembled Au/Pd/Au nanowires were sensitive toward hydrogen gas at room temperature, with the detection limit of 0.5%.

5. Acknowledgements

We acknowledge the financial support from DMEA (Award No. DOD/DMEA-CNID H94003 – 06 – 02 – 0608). We also acknowledge Mr. Syed Mubeen and Ting Zhang for their assistance on sensor characterization.

6. References

[1] X. Duan, Y. Huang, R. Agarwal, C. M. Lieber, *Nature* **2003**, *421*, 241.
[2] Y. Xia, P. Yang, Y. Sun, B. Mayers, B. Gates, Y. Yin, F. Kim, H. Yan, *Adv. Mater.* **2003**, *15*, 353.
[3] H. He, N. J. Tao, *Encyclopedia of Nanoscience and Nanotechnology*, American Scientific Publishers, CA **2004**.
[4] P. A. Smith, C. D. Nordquist, T. N. Jackson, T. S. Mayer, B. R. Martin, J. Mbindyo, T. E. Mallouk, *Appl. Phys. Lett.* **2000**, *77*, 1399.
[5] X. Duan, Y. Huang, Y. Chi, J. Wang, C. M. Lieber, *Nature* **2001**, *409*, 66.
[6] K. Ramanathan, M. A. Banhar, M. Yun, W. Chen, A. Mulchandani, N. V. Myung, *Nano Lett.* **2005**, *4*, 1237.
[7] D. Whang, S. Jin, Y. Wu, C. M. Lieber, *Nano Lett.* **2003**, *3*, 1255.
[8] Y. Huang, X. W. Duan, C. M. Lieber, *Science* **2001**, *291*, 630.
[9] A. K. Bentley, J. S. Trethewey, A. B. Ellis, W. C. Crone, *Nano Lett.***2004**, *4*, 487.
[10] M. Tanase, D. M. Silevitch, A. Hultgren, L. A. Bauer, P. C. Searson, G. J. Meyer, D. H. Reich, *J. Appl. Phys.* **2002**, *91*, 8549.
[11] J. C. Love, A. R. Urbach, M. G. Prentiss, G. M. Whitesides, *J. Am. Chem. Soc.* **2003**, *125*, 12696.
[12] C. M. Hangarter, N. V. Myung, *Chem. Mater.* **2005**, *17*, 1320.
[13] M. Tanase, L. A. Bauer, A. Hultgren, D. M. Silevitch, L. Sun, D. H. Reich, P. C. Searson, G. J. Meyer, *Nano Lett.* **2001**, *1*, 155.
[14] J. J. Storhoff, R. Elghanian, R. C. Mucic, C. A. Mirkin, *J. Am. Chem. Soc.* **1998**, *120*, 1959.
[15] R. Elghanian, J. J. Storhoff, R. C. Mucic, R. L. Letsinger, C. A. Mirkin, *Science* **1997**, *277*, 1078.
[16] C. A. Mirkin, R. L. Letsinger, R. C. Mucic, J. J. Storhoff, *Nature* **1996**, *382*, 607.
[17] R. C. Mucic, J. J. Storhoff, C. A. Mirkin, R. L. Letsinger, *J. Am. Chem. Soc.* **1999**, *120*, 12674.
[18] G. P. Mitchell, C. A. Mirkin, R. L. Letsinger, *J. Am. Chem. Soc.* **1999**, *121*, 8122.
[19] B. Kannan, R. P. Kulkarni, A. Majumdar, *Nano Lett.* **2004**, *4*, 1521.
[20] J. K. N. Mbindyo, B. D. Reiss, B. R. Martin, C. D. Keating, M. J. Natan, T. E. Mallouk, *Adv. Mater.* **2001**, *13*, 249.
[21] A. Papra, N. Gadegaard, N. B. Larsen, *Langmuir* **2001**, *17*, 1457.
[22] J. H. Lee, H. B. Lee, J. D. Andrade, *Prog. Polm. Sci.* **1995**, *20*, 1043.
[23] M. Amiji, K. Park, *ACS Symp. Ser.* **1994**, *540*, 135.
[24] K. Fuchs, *Proc. Cambridge Philos. Soc.* **1938**, *34*, 100.
[25] E. H. Sondheimer, *Adv. Phys.* **1952**, *1*, 1.
[26] F. Mayadas, M. Shatzkes, *Phys. Rev. B* **1970**, *1*, 1382.
[27] W. Steinhogl, G. Schindler, G. Steinlesberger, M. Engelhardt, *Phys. Rev. B* **2002**, *66*, 075414.
[28] W. Steinhogl, G. Steinlesberger, M. Traving, M. Engelhardt, *J. Appl. Phys.* **2005**, *97*, 023706.
[29] J. Richter, M. Mertig, W. Pompe, H. Vinzelberg, *Appl. Phys. A* **2002**, *74*, 725.
[30] Zhang J, Wang X, Peng X, Zhang L, *Appl. Phys. A* **2002**, *75*, 485.
[31] C. Wang, A. Mandelis, J. A. Garcia, *Sens. Actuators B* **1999**, *60*, 228.
[32] V. G. Ponomareva, G. V. Lavrova, E. F. Hairetdinov, *Sens. Actuators B* **1997**, *40*, 95.

